Macromolecular Bioscience
www.mbs-journal.de

# γ-Butyrolactone Copolymerization with the Well-Documented Polymer Drug Carrier Poly(ethylene oxide)-*block*-poly(ε-caprolactone) to Fine-Tune Its Biorelevant Properties

*Tomáš Urbánek, Jiří Trousil, Dmytro Rak, Kristýna Gunár, Rafał Konefał, Miroslav Šlouf, Marián Sedlák, Olga Šebestová Janoušková, and Martin Hrubý**

**Polymeric drug carriers exhibit excellent properties that advance drug delivery systems. In particular, carriers based on poly(ethylene oxide)-*block*-poly(ε-caprolactone) are very useful in pharmacokinetics. In addition to their proven biocompatibility, there are several requirements for the efficacy of the polymeric drug carriers after internalization, e.g., nanoparticle behavior, cellular uptake, the rate of degradation, and cellular localization. The introduction of γ-butyrolactone units into the hydrophobic block enables the tuning of the abovementioned properties over a wide range. In this study, a relatively high content of γ-butyrolactone units with a reasonable yield of ≈60% is achieved by anionic ring-opening copolymerization using 1,5,7-triazabicyclo[4.4.0]dec-5-ene as a very efficient catalyst in the nonpolar environment of toluene with an incorporated γ-butyrolactone content of ≈30%. The content of γ-butyrolactone units can be easily modulated according to the feed ratio of the monomers. This method enables control over the rate of degradation so that when the content of γ-butyrolactone increases, the rate of degradation increases. These findings broaden the application possibilities of polyester-polyether-based nanoparticles for biomedical applications, such as drug delivery systems.**

## 1. Introduction

Amphiphilic polymeric nanoparticles (NPs) are nanomaterials generated by the self-association of polymeric amphiphiles above a critical aggregation concentration, and their use of intervention is based on their physicochemical properties and architecture; the array of hydrophilic and hydrophobic domains can vary.[1–3] A class of important biodegradable and/or biocompatible polymers, aliphatic polyesters, have been widely studied due to their large-scale accessibility by the ring-opening polymerization (ROP) of cyclic esters or lactones.[4] In contrast to the commonly used lactones or esters for the synthesis of aliphatic copolyesters, γ-butyrolactone (γBL) is a very promising monomer, as introduction of γBL into other aliphatic polyesters might modify the degradation rate to meet the desired application demand.[5–8] Notably, the biocompatibility of poly(γ-butyrolactone) (P4HB) has been shown to be better than that of poly(glycolic acid) and poly(lactide-*co*-glycolide), which are copolymers that have been widely studied in terms of drug delivery in vivo.[7,9] Given this, γBL has been suggested to be a suitable comonomer for drug delivery system tuning.

Although γBL seems to be the perfect choice as a monomer for polymers in medical applications, its thermodynamic parameters do not allow for it to undergo ROP to a sufficient extent.[10,11] In the 1930s, γBL was proclaimed as a nonpolymerizable substance[12] and the corresponding research slowed. Polymerization conditions have been considered the key factors that determine the polymerizability of a substance, and in the 1960s, γBL was successfully converted into low-molecular-weight polyester (1200–3500 g $mol^{-1}$) under extreme conditions (2 GPa, 165 °C);[13] the high-pressure homopolymerization of γBL has been reported several times, and the molecular weight was increased by acid catalysis.[14] Attempts were made to prepare high-molecular-weight P4HB under less extreme conditions, and in 2016, these attempts resulted in success when a lanthanum

T. Urbánek, J. Trousil, Dr. K. Gunár, Dr. R. Konefał, M. Šlouf, Dr. O. Šebestová Janoušková, Dr. M. Hrubý
Institute of Macromolecular Chemistry
Czech Academy of Sciences
Heyrovského náměstí 2, 162 00 Prague 6, Czechia
E-mail: mhruby@centrum.cz
J. Trousil
Department of Analytical Chemistry
Charles University
Faculty of Science
Hlavova 8, 128 43 Prague 2, Czechia
Dr. D. Rak, Dr. M. Sedlák
Institute of Experimental Physics
Slovak Academy of Sciences
Watsonova 47, 040 01 Košice, Slovakia
The ORCID identification number(s) for the author(s) of this article can be found under https://doi.org/10.1002/mabi.201900408.

**DOI: 10.1002/mabi.201900408**

 

complex was employed as a catalyst.[15] However, currently, as biologic and electronic applications are at the forefront of interest, the purity of polymers is taken into account, and thus, nonmetallic catalysts are preferred.[16–21] A viable strategy for the incorporation of γBL into a polymeric chain is its copolymerization with thermodynamically favorable monomers.[8,22,23]

Amphiphilic diblock copolymers composed of hydrophobic biodegradable polyester blocks and hydrophilic polymer blocks are very suitable for the construction of micellar/nanoparticle drug delivery systems with core-corona structures because hydrophobic drugs can be encapsulated into micelle cores, while the hydrophobic portion can be degraded into low-molecular-weight fragments after drug release, allowing for elimination from the system of the organism while the hydrophilic corona-forming block protects the core from unwanted interactions in the organism. Among such copolymers, methoxy poly(ethylene oxide)-*block*-poly(ε-caprolactone) is very popular for the construction of drug delivery systems. However, the tuning of its properties is limited by the chemical properties of the polymer block from which it is composed.

In this work, we report the synthesis and characterization of an amphiphilic block copolymer composed of mPEO and poly(ε-caprolactone-*co*-γ-butyrolactone) (PCL-*co*-P4HB) possessing a favorable amount of P4HB. This copolymer undergoes self-association in an aqueous medium and forms spherical amphiphilic assemblies, as determined by cryo-transmission electron microscopy (cryo-TEM). This intervention was found to be enzymatically degradable by two different approaches (dynamic light scattering, DLS, and flow cytometry) and noncytotoxic. In addition, the low-molecular-weight hydrolytic products of the polyester block (6-hydroxyhexanoic acid and 4-hydroxybutyric acid) are fully metabolizable into carbon dioxide and water. The novel copolymerization of P4HB into the hydrophobic polyester block of mPEO-PCL block copolymers of this article was found to be an excellent tool for the adjustment of the properties critical for its use in drug delivery systems (NP behavior, cell uptake, biodegradation rate, and intracellular localization) over a very wide range, strongly increasing the variety of possible uses.

## 2. Experimental Section

### 2.1. Materials

γBL (≥99%) and ε-caprolactone (εCL, 97%) were purchased from Sigma-Aldrich Ltd. (Prague, Czechia), dried over calcium hydride for 24 h, subsequently distilled under reduced pressure, and stored under an inert atmosphere prior to use.

Benzyl alcohol (BA, ≥99%, Sigma-Aldrich Ltd.) was dried over calcium oxide for 24 h and subsequently distilled under reduced pressure twice and stored under an inert atmosphere prior to use. Poly(ethylene oxide) monomethyl ether, 2 and 5 kDa ($mPEO_{45}$ and $mPEO_{114}$, Sigma-Aldrich Ltd.), were azeotropically dried with toluene prior to use.

3,5-Bis(trifluoromethyl)phenyl isothiocyanate (98%), 1-(4,5-dimethylthiazol-2-yl)-3,5-diphenylformazan (MTT, BioReagent), cyclohexylamine (≥99.9%), 1,8-diazabicyclo[5.4.0]undec-7-ene (DBU), diphenyl phosphate (DPP), hydrochloric acid (in diethyl ether, 2 M), lipase from *Pseudomonas* sp. (type XIII) (Sigma-Aldrich Ltd.), paraformaldehyde, 1,5,7-triazabicyclo[4.4.0]dec-5-ene (TBD, 98%), 7-(diethylamino)coumarin-3-carbonyl azide (DACCA), and γ-hydroxybutyric acid sodium salt were purchased from Sigma-Aldrich Ltd. and used as received.

7-Aminoactinomycin D (7AAD), amphotericin B (250 μg $mL^{-1}$), CellMask Deep Red, Dulbecco's modified Eagle medium (DMEM, high glucose, GlutaMAX), fetal bovine serum (FBS, heat-inactivated), LysoTracker Deep Red, penicillin-streptomycin solution (10 000 U $mL^{-1}$), and Triton X-100 solution (1%) were purchased from Life Technologies Ltd. (Prague, Czechia).

### 2.2. Synthesis of *N*-(3,5-bistrifluoromethyl)phenyl-*N*′-cyclohexylthiourea (TU)

Cyclohexylamine (210 μL, 1.84 mmol) was added to 10 mL of dry dichloromethane (DCM) under an argon atmosphere. This solution was cooled in an ice bath and 3,5-bis(trifluoromethyl) phenyl isothiocyanate (337 μL, 1.85 mmol) was added.[24] The reaction was maintained overnight (16 h) at room temperature. The product precipitated from the solution, the solvent was evaporated under reduced pressure and the product was purified by recrystallization from petroleum ether with a yield of 91%. The product was further used as a cocatalyst of DBU for the ROP of γBL with εCL.

### 2.3. Synthesis of Poly(ε-caprolactone-*co*-γ-butyrolactone) (PCL-*co*-P4HB)

Polymerization reactions (**Figure 1**A) were carried out in dry vessels under an argon atmosphere for 24 h. The desired amounts of initiator (BA), catalyst ($HCl/Et_2O$, DPP, TBD or DBU/TU), and solvent were added into the vessels equipped with magnetic stirring bars. The solutions were stirred while the monomers (εCL and γBL) were added. The feed ratios are listed in the Tables S1 and S2 in the Supporting Information. The products were washed with ice-cold $Et_2O$.

### 2.4. Synthesis of Poly[ethylene oxide-*block*-(ε-caprolactone-*co*-γ-butyrolactone)] [mPEO-*b*-(PCL-*co*-P4HB)]

Polymerization reactions (Figure 1B) were carried out in the same manner as the polymerization of PCL-*co*-P4HB. In this case, the poly(ethylene oxide) monomethyl ethers were used as the macroinitiators and only TBD was used as the catalyst. Feed amounts are listed in Table S3 in the Supporting Information.

### 2.5. Fluorescent Labeling of mPEO-*b*-(PCL-*co*-P4HB)

Chosen samples of the prepared copolymers were labeled with DACCA for biological analysis, synthesis scheme shown in Figure S12 in the Supporting Information. Each sample of 80 mg of mPEO-*b*-(PCL-*co*-P4HB) was dissolved in 10 mL of toluene, and 2 molar equivalents of DACCA were added to this

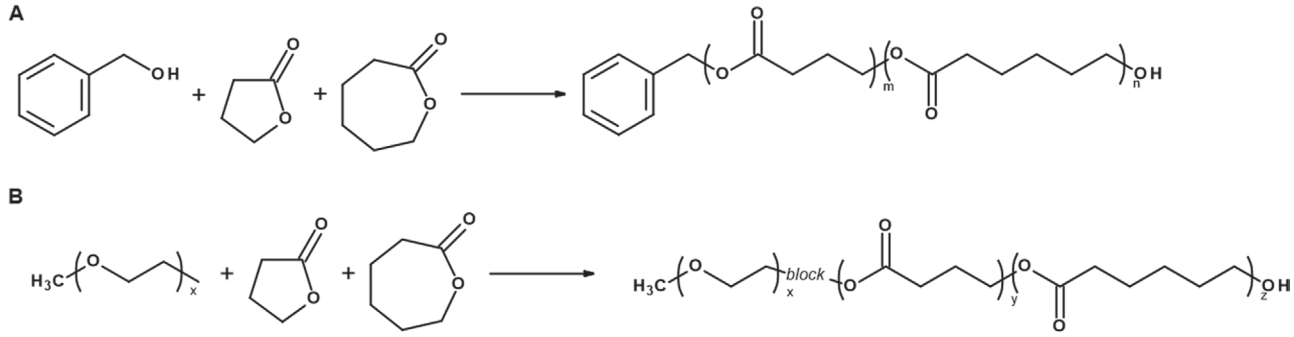


**Figure 1.** Synthesis scheme of A) copolymer PCL-*co*-P4HB and B) block copolymer mPEO-*b*-(PCL-*co*-P4HB).

solution. The reactions were maintained at 80 °C under an argon atmosphere for 24 h.[25] The products were purified by dialysis and freeze-dried. The UV–vis spectra were measured with a UV–vis spectrophotometer (Evolution 220 Spectrometer, Thermo Scientific, USA). Fluorescence spectra of the samples were recorded (90° angle geometry, 1 × 1 cm quartz cell) with an Aminco Bowman Series 2 spectrofluorometer (Aminco, Lake Forest, CA, USA) at an excitation wavelength of 420 nm and are shown in Figure S13 in the Supporting Information.

### 2.6. Preparation of Nanoformulations

Nanoparticles were prepared by the nanoprecipitation method. Samples of mPEO-*b*-(PCL-*co*-P4HB) (10 mg) were diluted in acetone (1 mL), and subsequently, an aqueous phase [distilled water or phosphate-buffered saline (PBS)] (10 mL) was rapidly added while stirring at 200 rpm. The excess acetone was evaporated under reduced pressure. The final concentrations of the samples were 1 mg $mL^{-1}$. Nanoformulations were always prepared fresh for each characterization.

### 2.7. Characterization of PCL-*co*-P4HB and mPEO-*b*-(PCL-*co*-P4HB)

Proton nuclear magnetic resonance ($^1$H NMR), size-exclusion chromatography (SEC), and Fourier transform infrared spectroscopy (FTIR) were used for fundamental characterization of the synthetized copolymer structures.

A Bruker AVANCE DPX 300 (and/or AVANCE III 600 MHz) spectrometer (Bruker Daltonik GmbH, Bremen, Germany) operating at 300.1 or 600.2 MHz was utilized for chemical structure determination. All samples were dissolved in deuterated chloroform at 25 °C. The chemical shifts were relative to tetramethylsilane (TMS) using hexamethyldisiloxane (HMDSO, $\delta$ = 0.05 ppm from TMS) as the internal standard.[26] $^{13}$C NMR spectrum was recorded using Bruker AVANCE III 600 MHz operating at 150.9 MHz in deuterated chloroform at 25 °C. The chemical shift was relative to TMS using HMDSO ($\delta$ = 2.00 ppm from TMS) as the internal standard.

A Perkin Elmer PARAGON 1000 PC FTIR spectrometer was utilized for chemical structure confirmation. The spectrometer had a resolution of 4 $cm^{-1}$, 32 accumulated scams, and strong apodization. The reflective measurements were performed using an ATR-Specac MKII Golden Gate Single Reflection system with a diamond crystal and an angle of incidence of 45°. The samples were characterized in powder form.

Physical characterization of the synthetized copolymers was determined by SEC. Namely, the mass-average molar mass $M_n$, the number-average molar mass $M_w$, and their ratio $M_w/M_n$ provided information about the chain length distribution–dispersity, $Đ$. The separation was carried out using a DeltaChrom pump (Watrex Ltd., Prague, Czechia), a Midas Spark autosampler (DataApex Ltd., Prague, Czechia), and two PLgel MIXED-B-LS columns. The samples were dissolved in tetrahydrofuran (THF), which served as the mobile phase in the chromatographic system with a flow rate of 1 mL $min^{-1}$ at 25 °C. A PL ELS-1000 evaporative light scattering detector (Polymer Laboratories, Varian Inc., Amherst, USA) was used for the detection. The evaluation of the sample chromatograms was performed using Clarity Software Version 6.0.0.295 (DataApex Ltd.) with polystyrene standard calibration.[27]

### 2.8. Characterization of the Nanoparticles Prepared by mPEO-*b*-(PCL-*co*-P4HB)

Different techniques were used for the characterization of the nanoparticles. DLS measurements were carried out on a ZEN3600 Nano-ZS instrument (Malvern Instruments Ltd., UK) using an angle of 173°. A He–Ne laser (4.0 mW, operating at 633 nm) was used. The hydrodynamic diameter of the particles was calculated from the diffusion coefficient using the Stokes–Einstein equation.

Static light scattering (SLS) measurements were performed on an ALV-6010 instrument (ALV GmbH, Germany) equipped with a 22 mW He–Ne laser in the angular range of 30°–150°. The data were analyzed by using a Zimm plot. The d$n$/d$c$ values were measured as described below.

The additional method for characterizing the prepared nanoparticles was asymmetric-flow field-flow fractionation (AF4). The instrument setup for AF4 consisted of an Eclipse 3+ separation system (Wyatt Technology Europe, Dernbach, Germany) coupled to a 1260 Infinity isocratic pump and degasser (Agilent Technologies, Santa Clara, CA, USA), a DAWN HELEOS II MALS detector with a 120 mW gallium-arsenide laser at a wavelength of 661 nm (Wyatt Technology, Santa Barbara, CA, USA), and an RI-101 RI detector (Shodex, Munich, Germany). Prepared nanoparticles in filtered

deionized water underwent measurements using a 275 mm long trapezoidal channel consisting of a 490 µm spacer and a regenerated cellulose membrane with a 5 kDa cutoff. Collected data were processed using ASTRA 6 software.

The measurements followed the established procedure in ref. [28]. As a result, the mass-average molar mass $M_w$ and the diameter of gyration $D_g$ were obtained.

The refractive index increment d$n$/d$c$ of the solutions was measured with a BI-DNDCW differential refractometer (Brookhaven Instruments Corporation, USA). The d$n$/d$c$ values were obtained using a potassium chloride calibration solution.

### 2.9. Morphology of the NPs

The nanoparticle morphology was observed by transmission electron microscopy. To characterize the morphology of the nanoparticles, 3 µL of sample solution was applied to a formvar-carbon electron microscopy grid. Samples were observed without staining at 100 kV using an FEI Morgagni TEM equipped with a MegaView III side-entry charge-coupled device camera. For cryo-TEM, where the hydrated samples were imaged without the perturbation generated by drying, the sample solution was applied to a carbon-covered polymer-grid supporting film (lacey-carbon grids, Electron Microscopy Sciences, Hatfield, USA) and glow discharged for 40 s with a 5 mA current. Most of the sample was removed by blotting and the grid was immediately plunged into liquid ethane at –183 °C. The sample was then transferred without rewarming into a Tecnai Sphera G20 electron microscope (FEI) using a Gatan 626 cryo-specimen holder (Gatan Inc., Pleasanton, CA, USA). Images were recorded at a 120 kV accelerating voltage using a Gatan UltraScan 1000 slow-scan charge-coupled device camera (achieving a final pixel size from 2 to 0.7 nm) in low-dose mode.

### 2.10. Enzymatic Degradation of NPs

The $^1$H NMR and SEC measurements were used to determine the enzymatic degradation of the prepared nanoparticles and the procedure is described in ref. [28]. The degradation was studied in the presence of lipase from *Pseudomonas* sp. The appropriate amount of lipase (aqueous solution in PBS, 4 U mL$^{-1}$) was added to the nanoformulation (1 mg mL$^{-1}$ in PBS) to initiate the degradation process, giving final concentrations of the copolymer and lipase of 0.98 mg mL$^{-1}$ and 0.06 U mL$^{-1}$, respectively. The degradation was performed at 37 °C inside an NMR cuvette. In case of SEC measurements, the purification of the organic content was needed to be done after the degradation period. The PBS solution of the sample incubated with the lipase was poured into excess of cold diethyl ether, so the organic content precipitated. The precipitate was separated by centrifugation at 7000 rpm and 0 °C and dried. This material was dissolved in mobile phase of SEC and the analysis was performed.

### 2.11. Critical Aggregation Concentration (CAC) Determination

The NP formulations of the synthesized copolymers were prepared by the protocol described above. Series of concentrations reaching 10$^{-6}$ mg mL$^{-1}$ were obtained by serial dilution in PBS. A solution of Nile red in ethanol was added to each sample to obtain a final concentration of 10$^{-6}$ mol L$^{-1}$. A Synergy H1 Hybrid Reader instrument (BioTek, Winooski, USA) was utilized to record the fluorescence of the samples. The excitation wavelength was 550 nm and the emission intensity was measured at 650 nm. The CACs were determined as the intersection points of the lines from two different parts of the graph of fluorescence intensity versus the negative logarithm of the concentrations, as seen in Figure S8 in the Supporting Information.[28]

### 2.12. Hemolysis assay

The determination of blood compatibility with the prepared NPs was carried out following the procedure in ref. [28]. Fresh human blood was collected for the analysis into heparin-coated vacutainers (Becton Dickinson Czechia Ltd., Prague, Czechia). Red blood cells (RBCs) were obtained by centrifugation of the blood at 3000 rpm for 10 min. The plasma was removed and RBCs were washed with PBS. The final concentration of RBCs in PBS for the hemolysis measurements was at a full blood dilution of 1:49.

To 0.3 mL of diluted RBCs, 1.2 mL of the appropriately diluted nanoformulation (in PBS) was added. With this procedure, several dilutions of NPs were prepared (100, 200, 400, and 800 µg mL$^{-1}$). Triton X-100 (1% in PBS) and PBS served as positive and negative controls, respectively.

After incubation at 37 °C for 8 h, the samples were centrifuged (3000 rpm, 10 min). Subsequently, the supernatants were collected and subjected to absorbance measurement at 541 nm on a Synergy H1 Hybrid Reader instrument (BioTek, Winooski, Vermont, USA). The percent hemolysis of RBCs in each sample was calculated by the following Equation (1)

$$\text{Hemolysis} = \frac{\text{sample absorbance} - \text{negative control}}{\text{positive control} - \text{negative control}} \times 100 \quad (1)$$

The results of the hemolysis assays were expressed as a percentage of the positive control (1% Triton X-100 in PBS), which was considered 100%. Hemoglobin release up to 2% was classified as nonhemolytic, according to the ASTM F756-08 standard.[29] The results of this assay are expressed as mean values of triplicate analysis.

### 2.13. Cell Culture

The murine monocyte-macrophage (M$\phi$) cell line J774A.1[30] was purchased from Sigma-Aldrich Ltd. The cells were maintained in DMEM supplemented with FBS (10%), penicillin (100 U mL$^{-1}$), streptomycin (100 µg mL$^{-1}$), and amphotericin B (2.5 µg mL$^{-1}$) in a humidified atmosphere containing 5% $CO_2$ at 37 °C.

### 2.14. Cytotoxicity Study

Cytotoxicity was evaluated using the MTT assay. For this purpose, J774A.1 M$\phi$s were seeded in 96-well plates at a density of 5000 cells per well. The cells were then incubated overnight at 37 °C and 5%

$CO_2$ with subsequent replacement of the medium with 100 µL of fresh culture medium containing the tested formulations. After 24 h of incubation, the medium was replaced with 100 µL of MTT solution (0.5 mg $mL^{-1}$ in PBS), and the plates were incubated for 2–4 h prior to aspiration of the medium and dimethyl sulfoxide addition (100 µL). After 15 min of blue formazan solubilization (37 °C), a Synergy H1 Hybrid Reader instrument (Biotek, Winooski, USA) was used to assess cell viability by spectrophotometry at 570 nm. The results of the MTT assay were expressed as a percent of the control (cells in control medium), which was considered 100 %. A reduction in cell viability by more than 30% was considered a cytotoxic effect according to the ISO 10993-5.[31] The tests were performed in at least three separate experiments.

### 2.15. Microscopic Investigation of Cellular Uptake

Confocal laser scanning microscopy (CLSM) was used to study cellular uptake and lysosome-nanoparticle colocalization. For the uptake study, J774A.1 cells were seeded at the bottom of ibidi µ-dishes (ibidi GmbH, Planegg/Martinsried, Germany) and left to adhere overnight. Subsequently, the medium was replaced with fresh medium (full DMEM) containing DACCA-labeled NPs (2.8 nmol $mL^{-1}$). After 40 min of incubation, the cells were washed with prewarmed PBS (37 °C) three times, stained with CellMask Deep Red according to the manufacturer's protocol for 10 min, washed with warm PBS, fixed using a paraformaldehyde solution (4% in PBS), and kept under PBS until subsequent analysis. Cells were visualized on an Olympus FV 10 confocal laser scanning microscope (Olympus Czech Group Ltd., Prague, Czech Republic) using a 60 × oil objective. Signal detection was observed in channels 1 (DACCA, exc. 405 nm, em. 425–475 nm) and 2 (CellMask Deep Red, exc. 650 nm, em. 655–750 nm).

Similarly, the lysosome-nanoparticle colocalization study was carried out using overnight-adhered macrophages (M$\phi$s). The medium was replaced with fresh DMEM containing DACCA-labeled NPs (2.8 nmol $mL^{-1}$) and LysoTracker ($0.0125 \times 10^{-6}$ M) and incubated for 40 min. Subsequently, the cells were washed and fixed as described above. Visualization was carried out using the same instrument under the same conditions. Before image analysis, the images were converted to eight-bit grayscale pictures, and the levels of colocalization were determined using ImageJ software. An image of the product of the differences from the mean (PDM), i.e., for each pixel: (blue intensity − mean blue intensity) × (red intensity − mean red intensity), was used to analyze the colocalization. In addition, Pearson correlation coefficient (PCC) values were calculated using the same software. For this purpose, at least six fields were used for the PCC calculation. PCC is a positive correlation between different channels that generates values ranging from −1 to 1. A value of 1 suggests a perfect positive linear correlation. Hence, in this case, a value of 1 would indicate total colocalization of the DACCA-labeled nanobead-based intervention with LysoTracker-positive compartments.

### 2.16. Flow Cytometry Investigations

Cellular internalization and intracellular degradation were studied by flow cytometry. Cell uptake of the fabricated DACCA-labeled NPs was measured via a BD FACSVerse flow cytometer (BD Biosciences, Franklin Lakes, NJ, USA). For this purpose, J774A.1 cells were incubated at 37 °C and 5% $CO_2$ in full DMEM. The overnight culture was seeded at a density of 200 000 cells per sample. NPs were added at a final concentration of 2 nmol $mL^{-1}$ to the wells and incubated for 1, 5, 20, 40, 60, or 80 min. After washing with warm PBS, the cells were suspended in 0.5% bovine serum albumin (BSA, in PBS solution). Dead cells were stained with 7AAD according to the manufacturer's protocol. The measurement was repeated independently three times and in duplicate. Cell-associated fluorescence was analyzed using FlowJo 10.5.0 software (Tree Star Inc., Ashland, OR, USA).

Intracellular degradation estimation was based on a previously described method.[28] The overnight J774A.1 culture was seeded at a density of 200 000 cells per sample. NPs at a concentration of 2 nmol $mL^{-1}$ were added to the appropriate wells and incubated for 60 min in full DMEM (37 °C, 5% $CO_2$). The incubation length was chosen according to the above-described internalization-related experiment, where the macrophages showed the maximum internalized NPs between 60 and 80 min of incubation. After washing with warm PBS, the cells were further incubated in particle-free full DMEM for 0, 10, 20, 30, 40, or 80 min. Cells were washed with PBS and suspended in 0.5% BSA (PBS solution); dead cells were stained with 7AAD and measured by BD FACSVerse. The measurement was repeated independently three times and in duplicate. Cell-associated fluorescence was analyzed using FlowJo 10.5.0 software.

## 3. Results and Discussion

### 3.1. Synthesis and Content of 4HB in PCL-*co*-P4HB

Previous studies that have focused on the polymerization of five-membered lactones have shown their unwillingness to undergo ring-opening polymerizations due to the low ceiling temperature.[10] However, this does not mean that the ring of five-membered lactones cannot be opened and that only the cyclic form is thermodynamically preferred. These rings do open, but there is no impetus to form high-molecular-weight polymers under normal conditions.[32,33] This is the reason why these compounds are difficult to homopolymerize but, on the other hand, are easy to incorporate into a polymer chain when copolymerization occurs with another appropriate heterocycle with a high ceiling temperature. Moreover, the extent of incorporation can also be tuned by the polymerization conditions.[10,34]

Hence, for the systematic investigation of incorporating $\gamma$BL into polymer chains during copolymerization with $\varepsilon$CL, a series of copolymerizations initiated by benzyl alcohol were performed (Figure 1A) with different copolymerization conditions. The polymerization parameters and resulting characterizations are given in Tables S1 and S2 in the Supporting Information. The data in Table S1 in the Supporting Information show the parameters depending on the feed ratio of monomers, whereas the data in Table 2 show the parameters depending on the nature of the catalyst and the solvent and the initial monomer concentrations. In total, four different catalytic systems were evaluated (structures shown in **Figure 2**A).

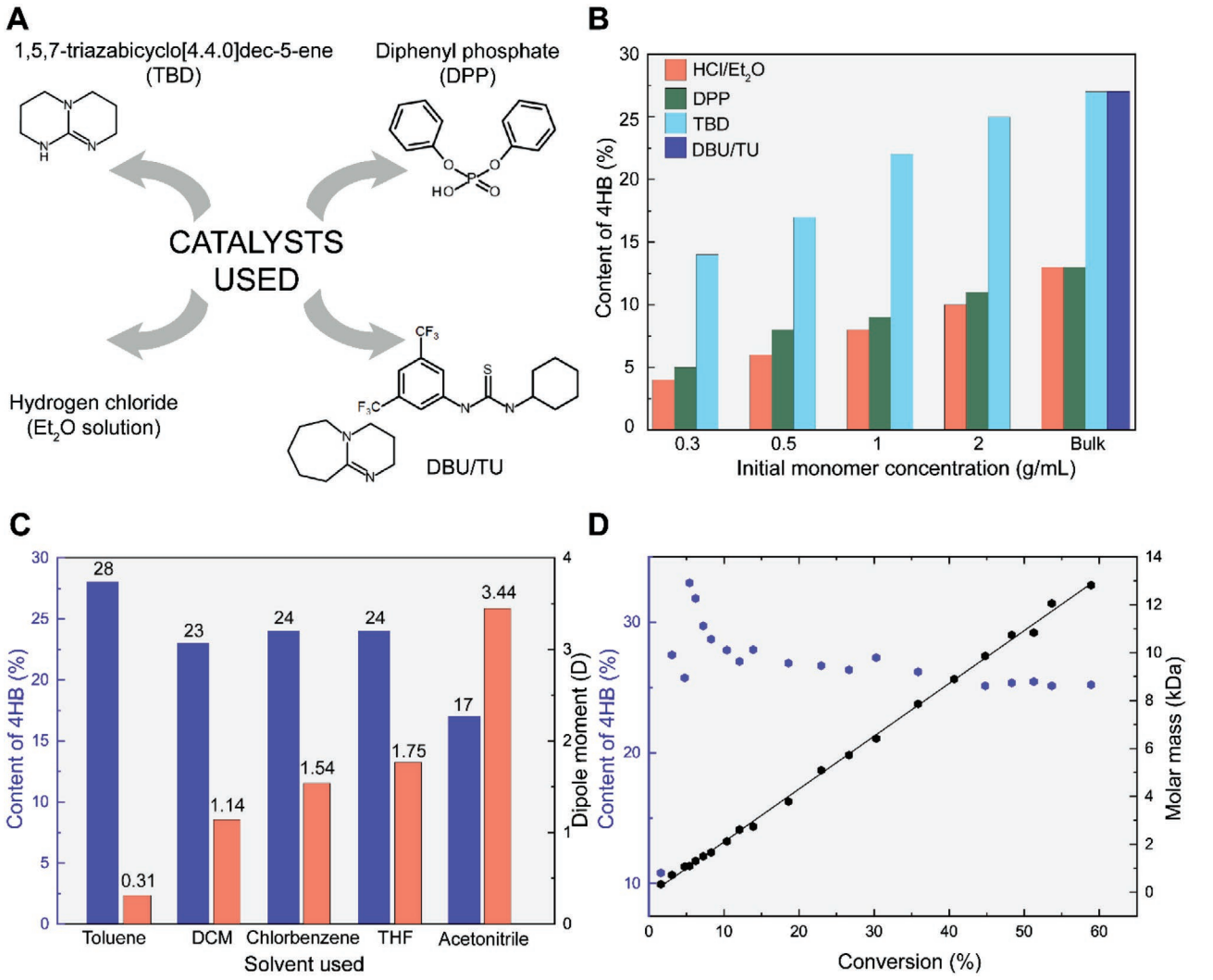


**Figure 2.** Copolymerization optimization. A) Different catalysts were used in subsequent studies of the content of 4HB in copolymers. B) Different initial monomer concentrations with DCM as the solvent as well as C) different solvents possessing various dipole moments were studied with TBD used the catalyst. D) The relationship between monomer consumption and the content of 4HB in the polymer chain and molar mass was studied. The $\varepsilon$CL/$\gamma$BL molar feed ratio was in all cases 1.15. Abbreviations: TBD, 1,5,7-triazabicyclo[4.4.0]dec-5-ene; DPP, diphenyl phosphate; $Et_2O$, diethyl ether; DBU, 1,8-diazabicyclo[5.4.0]undec-7-ene; TU, *N*-(3,5-bistrifluoromethyl)phenyl-*N*′-cyclohexylthiourea; DCM, dichloromethane; THF, tetrahydrofuran.

The data in Table S1 in the Supporting Information show the relationship between the monomer feed ratio and the amount of incorporated $\gamma$BL. Not surprisingly, the higher the ratio of $\gamma$BL in the feed, the more $\gamma$BL was incorporated. The disadvantage of copolymerization with high amounts of $\gamma$BL is its relatively low yield. The difference in the incorporated amount of $\gamma$BL is remarkable when different catalysts were used (**P1–P4** catalyzed by HCl/Et2O and **P5–P8** by TBD).

The data schematically plotted in Figure 2B show a significant difference in the incorporated amount of $\gamma$BL when different catalysts were used. A higher content of 4HB units in the prepared copolymers was observed when anionic catalysts (TBD and DBU/TU) were used compared to that observed in the copolymers prepared with cationic catalysts ($HCl/Et_2O$ and DPP). This fact implies that different polymerization mechanisms significantly affect the amount of incorporated $\gamma$BL.

The bulk copolymerization catalyzed by DBU/TU resulted in a yield of 39% and a copolymer containing 27% 4HB units but there was no high-molecular-weight copolymer formed when solution copolymerization was carried out at any concentration. TBD was identified as the most efficient and versatile catalytic system in this study. TBD is able to incorporate a relatively high amount of $\gamma$BL at any initial monomer concentration. The trend of increasing incorporated $\gamma$BL amount with increasing initial monomer concentration is evident in Figure 2B.

Solvent polarity is a considerable parameter when a certain amount of $\gamma$BL incorporation is needed in the polymer chain. As shown in Figure 2C, there was a marked difference in 4HB content in the copolymer composition of PCL-*co*-P4HB when the nonpolar solvent toluene was used compared to the 4HB content when polar acetonitrile was used. It should be noted that TBD is a bifunctional catalyst, in which the base site works as a H-bonding acceptor to activate the alcohol initiator, while

the H-bonding donor component can activate the monomer via the coordination of the ester functionality. Thus, the noncoordinating solvent toluene enables higher incorporation of γBL in the evaluated copolymerization reaction.

The prepared copolymers were characterized by $^1$H NMR and FTIR spectroscopy, and their structures were confirmed. The $^1$H NMR spectra and FTIR spectra are shown in Figures S2 and S3 in the Supporting Information, respectively. The table of polymerization parameters and copolymer characteristics obtained by $^1$H NMR spectroscopy and size exclusion chromatography can be found in Table S2 in the Supporting Information.

In addition, a $^1$H NMR spectroscopic kinetic study was performed to understand the copolymerization behavior. TBD was used as the catalyst for this purpose and deuterated DCM was used as the solvent. The polymerization was performed in an NMR cuvette in situ and $^1$H NMR spectra were taken periodically over time. The relative intensities of peaks corresponding to the γBL unit ($\delta$ 1.91 ppm) and the εCL unit ($\delta$ 1.33 ppm) were integrated and the following parameters were calculated. The resulting graph in Figure 2D shows the dependence of the content of 4HB and molar mass on the conversion. A moderate decrease in the content of 4HB units in the growing polymer chain with increasing conversion was observed, and the linear dependence of molar mass on conversion indicated the controlled manner of ring opening copolymerization. Additionally, the rate constants of the incorporation of γBL and εCL were determined. As the graphs in Figure S7 in the Supporting Information of the supplemental information show, εCL has been incorporated according to first-order kinetics with a rate constant of $k_{\varepsilon CL} = 4.3 \times 10^{-5}$ s$^{-1}$, and the incorporation of γBL follows second-order kinetics with a rate constant of $k_{\gamma BL} = 5.8 \times 10^{-6}$ dm$^3$ mol$^{-1}$ s$^{-1}$.

### 3.2. Synthesis of mPEO-*b*-(PCL-*co*-P4HB)

Many studies have shown that assemblies based on poly(ethylene oxide)-*block*-polycaprolactone can be successfully used as drug carriers for many medical applications.[35,36] Copolymerization with mPEO and other hydrophilic polymers ensures or enhances the solubility of these assemblies based on the copolymers and improves the biocompatibility/nonimmunogenicity of the whole system.[37] When mPEO is used for copolymerization, the assemblies do not show any toxicity at reasonable concentrations and are efficient when loaded with hydrophobic drugs,[27] suggesting an attractive polymeric matrix for drug delivery system preparation.

Thus, this work aimed to study the impact of 4HB disturbance on hydrophobic block regularity and on the biorelevant properties of mPEO-based assemblies. Given this, the most efficient conditions for incorporating γBL via the copolymerization initiated by BA were implemented (see above) and the copolymerization was conducted via ROP in the same manner and in the presence of the macroinitiator mPEO (Figure 1B). The macromolecular parameters of the prepared block copolymers are listed in **Table 1**. Samples **B2**–**B5** differ in hydrophobic ratio and macromolecular molar mass (i.e., mPEO) and in the molar mass of the samples themselves. The $^1$H NMR spectrum of mPEO-*b*-(PCL-*co*-P4HB) with signal assignment is shown in Figure S6 in the Supporting Information. Moreover, the $^{13}$C NMR spectrum in Figure S14 in the Supporting Information gave as detailed information about the copolymer microstructure. It proved that the distribution of CL and 4HB units along polyester block is very likely random.[38]

Sample $mPEO_{44}$-*b*-$PCL_{81}$ **B1** was synthesized in the absence of γBL for comparison of the properties with those of samples **B2** and **B3**. The critical aggregation concentrations were determined and the values are listed in Table 1. The CAC-related curves are shown in Figure S8 in the Supporting Information.

The one-step synthesis of labeled mPEO-*b*-(PCL-*co*-P4HB) with fluorescent dye was performed. DACCA was used for this purpose and the reaction scheme is shown in Figure S12 in the Supporting Information. The efficiencies of the reactions were determined by the standard addition method (free 7-(diethylamino)coumarin-3-carboxylic acid) and were found to be ≈45% by UV–vis spectroscopy. The absolute amounts of DACCA occurring in the polymeric matrices are listed in Table 1. The excitation and emission spectra at the excitation wavelength of 420 nm of free 7-(diethylamino)coumarin-3-carboxylic acid and samples of **B1**–**B5** are shown in Figure S13 in the Supporting Information.

### 3.3. Characterization of the Nanoparticles

The fabricated copolymers (**B1**–**B5**) were used for NP preparation. For this purpose, the nanoprecipitation method described

**Table 1.** Composition and characteristics of polymers initiated by poly(ethylene oxide) monomethyl ether (mPEO) using TBD as the catalyst.

| No. | Copolymer | HH-ratio[a)] | Yield [%] | $f_{\gamma BL}$[b)] [%] | $M_n^{NMRc)}$ | $M_n^{SECd)}$ | $Đ^{SECd)}$ | CAC[e)] [μg mL$^{-1}$] | DACCA[f)] [μg mg$^{-1}$] |
|---|---|---|---|---|---|---|---|---|---|
| B1 | $mPEO_{45}$-*b*-$PCL_{81}$ | 4.6 | 92 | 0 | 11 200 | 8300 | 1.21 | 9 | 20 |
| B2 | $mPEO_{45}$-*b*-($PCL_{39}$-*co*-$P4HB_{13}$) | 2.8 | 62 | 20 | 7500 | 6700 | 1.45 | 15 | 9 |
| B3 | $mPEO_{45}$-*b*-($PCL_{55}$-*co*-$P4HB_{19}$) | 4.0 | 60 | 21 | 9900 | 10 500 | 1.58 | 11 | 10 |
| B4 | $mPEO_{114}$-*b*-($PCL_{41}$-*co*-$P4HB_{12}$) | 1.1 | 63 | 18 | 10 800 | 7600 | 1.25 | 14 | 7 |
| B5 | $mPEO_{114}$-*b*-($PCL_{124}$-*co*-$P4HB_{45}$) | 3.6 | 59 | 21 | 23 000 | 12 300 | 1.61 | 10 | 4 |

[a)]The hydrophobic ratio was defined as ($M_n$, hydrophobic block)/($M_n$, hydrophilic block), where the $M_n$ of the hydrophilic block was held at either 2000 or 5000 depending on which macroinitiator was used; [b)]The polymer composition ratios of hydrophobic blocks were calculated using $^1$H NMR data by dividing the integrated peaks of the repeating unit of γBL ($\delta$ 1.95 ppm) by the sum of the integrated peaks of γBL and εCL ($\delta$ 1.37 ppm); [c)]The molecular weights were calculated using $^1$H NMR by integrating the methoxy peak of mPEO at 3.37 ppm and the peak for the repeating units of εCL and γBL; [d)]Determined by SEC using tetrahydrofuran as the eluent; [e)]Critical aggregation concentrations were determined at room temperature in PBS; [f)]When DACCA-labeled copolymers were used, the content of DACCA was determined by UV–vis spectroscopy.

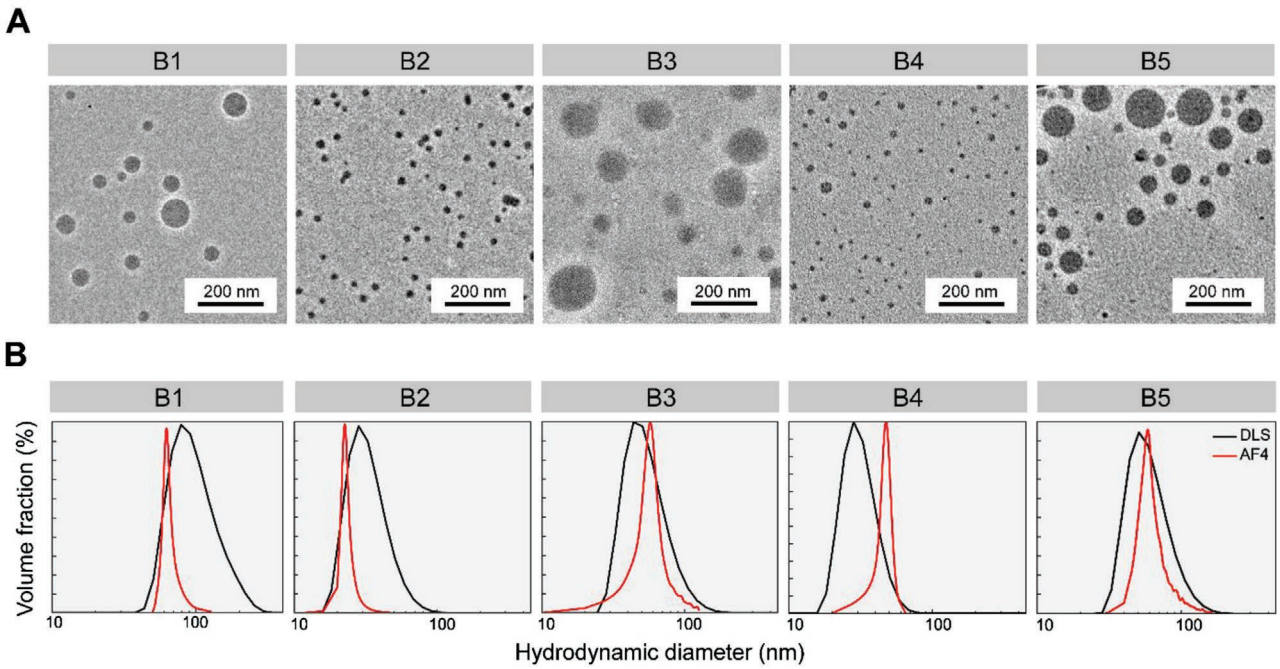


**Figure 3.** A) Cryo-TEM images and B) curves obtained from DLS and AF4.

in detail in the Experimental Section was used. The physicochemical characterization of the NPs was performed via cryo-TEM, DLS, SLS, and AF4 experiments.

It was hypothesized that the supramolecular structure of the mPEO-*b*-(PCL-*co*-P4HB)-based assemblies correlated to the structure of mPEO-*b*-PCL in some respects, as the only difference was the aliphatic chain length between the ester bonds in the repeating units. In the context of mPEO-*b*-PCL assemblies, several architectures were described in the literature, depending on the hydrophobic/hydrophilic ratio.[35,39] Note that if the solvent switch is fast during NP preparation, block copolymers tend to form spherical structures instead of cylindrical or planar ones because this is the fastest way to reduce the interfacial area.[28] This is in line with the cryo-TEM investigations that revealed that all of the samples inspected were found to largely be spherical polymeric nanoparticles (**Figure 3**A) with diameters in mutual agreement with those found by DLS, SLS, and AF4 (**Table 2**).

The DLS distribution functions (Figure 3B) are portrayed as relatively narrow peaks, with diameters ranging from ≈40–110 nm depending on the block lengths. To verify these findings, we performed additional AF4 experiments that provided the actual sizes and molecular weights. These values are in mutual agreement with those obtained by DLS or SLS. It should be noted, however, that light scattering techniques usually overestimate the size of particles.[36,40] In addition, the samples for the AF4 measurements were filtered through large-pore polyvinylidene fluoride filters (0.8 µm), as AF4 is not as sensitive to dust as conventional light scattering techniques. Thus, any influence of filtration on the size distribution of the nanoparticles can be excluded.

The DLS and AF4 results together with the cryo-TEM investigations allowed for us to obtain insight into the structure of the NPs. In the literature,[39,41,42] mPEO-*b*-PCL-based assemblies are often stated to be micelles. The AF4-estimated molecular weight values (Table 2), however, indicate that ≈400–9000 polymer chains comprise one nanoparticle. Micelles, in contrast, contain ≈10–100 polymer chains.[43]

The apparent structural density ($\rho$) of the particles was calculated as an equivalent average density from the average of the

**Table 2.** Characterization of nanoparticles.

| Sample | $D_H^{DLS}$ a) [nm] | PDI a) DLS | $D_G^{SLS}$ b) [nm] | $M_W^{SLS}$ b) [kDa] | $\rho^{SLS}$ c) [g mL$^{-1}$] | $D_G^{AF4}$ b) [nm] | $M_W^{AF4}$ b) [kDa] | $\rho^{AF4}$ c) [g mL$^{-1}$] | $N_{agg}^{AF4}$ d) |
|---|---|---|---|---|---|---|---|---|---|
| B1 | 109 | 0.113 | 91 | 14 900 | 0.029 | 77 | 101 400 | 0.324 | 9050 |
| B2 | 41 | 0.188 | 40 | 5800 | 0.134 | 26 | 8160 | 0.690 | 710 |
| B3 | 71 | 0.166 | 120 | 13 800 | 0.012 | 85 | 24 700 | 0.060 | 1110 |
| B4 | 36 | 0.109 | 48 | 1000 | 0.013 | 47 | 4180 | 0.060 | 420 |
| B5 | 71 | 0.111 | 170 | 38 100 | 0.011 | 103 | 66 700 | 0.091 | 2510 |

a)The *Z*-average of the hydrodynamic diameter $D_H$ and polydispersity index PDI; b)The molecular weight $M_W$ and the *Z*-average of the diameter of gyration $D_G$; c)The apparent structural density was calculated from the equation $\rho = 6M_w/\pi N_A D^3$ considering a spherical shape ($D = 1.29 \cdot D_G$); d)The aggregation number is the quotient of the $M_W$ of the particles (AF4) and the $M_W$ of the polymer (SEC).

molecular weight $M_w$ using the model of a sphere with a diameter of $D = 1.29\ D_G$; therefore, $\rho = 6M_w/\pi N_A D^3$. On average, the density of the mPEO-*b*-(PCL-*co*-P4HB) nanoparticles was three times lower than the density of the mPEO-*b*-PCL nanoparticles. Given this finding, we hypothesized that the 4HB-possessing NPs were less dense due to their irregular structure (two repeating units) within the hydrophobic core. This also means that the core of the mPEO-*b*-(PCL-*co*-P4HB) nanoparticles was less hydrophobic than that of the mPEO-*b*-PCL nanoparticles, which may influence cargo encapsulation. However, this issue was not addressed further.

One of the advantages of the AF4 method over conventional light scattering methods or cryo-TEM is the capability of AF4 to detect eventual nonassembled polymers in solution. The AF4 investigations revealed that no free nonassembled polymer was found in any of the samples investigated in this work. This is probably due to the favorably low estimated CAC values (i.e., 9–15 μg $mL^{-1}$) and supports the above-discussed fact that our assemblies are not micelles, which are known to be in thermodynamic equilibrium with unimers, but instead are probably nanogel-like polymeric NPs.

The described complex characterization of NPs allowed for us to fine-tune the nanoparticle parameters so that the particles could be designed more precisely in the future according to the particular application requirements.

### 3.4. $^1$H NMR-Assessed Degradation

The enzyme-catalyzed degradation of the NPs was investigated using $^1$H NMR. The degradation was observed as a decrease in the intensity of the proton signal of ε-caprolactone units in sample **B1** and ε-caprolactone and γ-butyrolactone units in sample **B3** during the experiment. Samples **B1** and **B3** were chosen for this more detailed study due to the comparable sizes of the blocks in these copolymers. For the quantitative characterization of the enzymatic degradation of the PCL and PCL-*co*-P4HB blocks, the time dependence of PCL and PCL-*co*-P4HB consumption was calculated for the measured samples. The integral intensity of the signal marked as "g" (Figure S9, Supporting Information) was defined as 2 (there are two equivalent protons) and used as an internal standard for monitoring degradation in the NMR spectra. Subsequently, the integral intensity of the signal "i + l" (Figure S9, Supporting Information) was used to calculate the percentage of PCL and PCL-*co*-P4HB blocks according to the relationship $[(I_t^{i+l}/I_0^{i+l}) \times 100]$, where the subscripts 0 and $t$ represent the time points during degradation with $t = 0$ (i.e., before lipase addition) and $t = t$ (i.e., after lipase addition), respectively.

The results are shown in Figure S10 in the Supporting Information. It is evident that sample **B1** degraded faster than sample **B3**. Figure S9 in the Supporting Information shows the $^1$H NMR spectra of **B3**-based NPs that were measured in deuterated PBS at 37 °C before (A) and after (B, C) lipase addition. The chemical structures and signal assignments are presented in the same figure. The comparison between the spectra was recorded in a solvent suitable for all of the blocks (deuterated chloroform, cf. Figure S6, Supporting Information) and PBS (Figure S9, Supporting Information), showing that the broader signals obtained from the PCL-*co*-P4HB hydrophobic block and the strong signals obtained from the hydrophilic mPEO demonstrate the presence of core–shell formation in the deuterated PBS system. These results demonstrate that the PCL-*co*-P4HB protons were restricted in mobility in the moderately hydrated solid-like core of the NPs, while the mPEO blocks created a liquid-like shell. After the addition of lipase, the intensity of the side methyl signals from the PCL-*co*-P4HB monomer unit ("i + l" and "j, e" protons, see Figure S9, Supporting Information) decreased, while the singlets related to the "f + h" and "k" protons split and the mPEO signals ("a", "b") remained unchanged. The second effect observed in this spectrum was the appearance of new signals related to the degradation products, which were identified as 6-hydroxyhexanoic acid and 4-hydroxybutanoic acid (Figure S9, Supporting Information).

Additionally, due to the appearance of the signals at 4.1, 2.2, and 2.0 ppm in Figure S9 in the Supporting Information, there was confirmation of an intermediate product during the degradation appeared before final the products (6-hydroxyhexanoic acid and 4-hydroxybutyric acid). From the chemical shifts of signals of this intermediate product, especially the peak at 4.1 ppm, which was shifted downfield to its respective signal from the polymer (i + l at 4.0 ppm), there was a high probability that this compound was a small cycle made from a small amount of CL and BL units. To support these considerations, one sample was chosen for $^1$H 2D diffusion-ordered NMR spectroscopy experiments, which were measured before lipase addition (Figure S11, Supporting Information red spectrum) and 24 h after lipase addition (Figure S11, Supporting Information blue spectrum). From those spectra it followed that the intermediate product was still not fully degraded after this time and had a slightly lower self-diffusion coefficient (higher molecular weight) than that of the final products (6-hydroxyhexanoic acid).

The degradation process of the copolymer was confirmed by SEC analysis. The products of degradation were collected in different times. As evident in Figure S15 in the Supporting Information, the degradation of the copolymer was already significant in the first hour of the action of the lipase.

### 3.5. Cytotoxicity Evaluation

To assess the biorelevant properties of the manufactured NPs, their cytotoxicity and hemolytic activity were analyzed in terms of their interactions with red blood cells (RBCs) and their behavior in monocyte-macrophage cultures, as these cells are one of the first contact partners after systemic administration. In addition, the goal of this evaluation was to answer the questions of whether our synthetized NPs are safe and whether the biocompatibility of P4HB-based assemblies is affected when P4HB is introduced within the Food and Drug Administration-approved mPEO-*b*-PCL copolymer.[44] The mPEO-*b*-PCL copolymer was found to possess no or only minor toxic effects on the cell viability of different cells, such as the murine monocyte-macrophage cell line Raw 264.7,[27,28] zebrafish embryonic fibroblast cell line ZF4,[28] human hepatocellular carcinoma cell line HepG2,[42,45] and prostate cancer cell lines LNCaP and PC-3.[46]

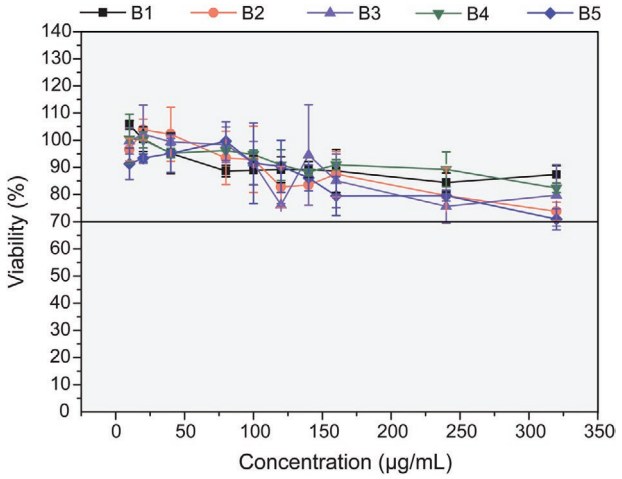


**Figure 4.** Viability of J774A.1 cells as detected by an MTT assay. Mϕs were incubated with different concentrations of the fabricated NPs for 24 h and their viability was analyzed via measurement of the concentration of metabolically produced formazan. The horizontal line in the panel indicates the level at which, in terms of cell viability, the distinction between cytotoxic (above) and noncytotoxic (below) was made.

First, we studied the effects of the prepared formulations **B1–B5** in terms of possible cytotoxicity by using the MTT method after a 24 h incubation of J774A.1 Mϕs with each prepared nanoformulation. As evident in **Figure 4**, the cell viability was influenced very little. The copolymer cytotoxicity was nearly negligible at clinically relevant concentrations. In the hemolytic study, none of the analyzed formulations (**B1–B5**) induced hemolysis within the tested concentration range (100–800 μg $mL^{-1}$) after an 8 h incubation at 37 °C.

Not surprisingly, the use of nanomedicines bears the risk of unwanted side effects.[44] Hence, an important step in the development of nanobead-based products is the assessment of any safety risks. Considering this, our results demonstrate that P4HB introduction within the copolymeric matrix did not affect its acute biocompatibility with both J774A.1 cells and RBCs.

### 3.6. Uptake and Intracellular Degradation Study

Our research group strives to rationally design nanobead-based interventions to benefit from the combination of the specific properties of NPs and those of biocompatible and biodegradable polymers in one self-assembled formulation allowing for drug delivery. Given this background, one of the crucial studied aspects was the question of whether the 4HB unit-possessing NPs could be taken up by J774A.1 Mϕs as a model cell type, which is an important subject of drug delivery research. Mϕs are the main hosts of intracellular pathogens and, thus, are pursued as a therapeutic target for the intracellular delivery of antibiotics. In addition, Mϕs have gained increasing interest as a therapeutic target for cancer immunotherapy due to its complex roles in the tumor microenvironment.[47]

The DACCA-labeled copolymers were visualized inside the J774A.1 cells using CLSM after an incubation time of 40 min. The microscopy study showed that all of the formulations tested, i.e., mPEO-*b*-PCL and mPEO-*b*-(PCL-*co*-P4HB), were successfully internalized in Mϕs (**Figure 5**), suggesting that such systems are usable as a logical strategy for effectively killing intracellular microbes.[48] Note that slight differences between the intracellular distribution patterns were evident. In other words, some of the samples revealed bright cytosolic localization (e.g., **B4**) compared to the vesicle-localized samples (e.g., **B1**). These findings seem to be in line with our previous mPEO-*b*-PCL-focused study,[28] which confirmed that control of the NP physicochemical properties also allows for control of their biorelevant behavior.

Given this, for a better view of the interactions between the NPs and J774A.1 cells, a marker for low pH compartments (i.e., presumably lysosomes) was applied to visualize the colocalization of the NPs. The cells were incubated for 40 min with DACCA-labeled NPs and LysoTracker Deep Red. These experiments indicated that all of the NP samples tested (**B1–B5**) were able to target acidic organelles (**Figure 6**), which was also proven by the analysis in terms of the PDM images and PCC value calculations. However, the DACCA-labeled nanoparticle colocalization with lysosomes was not found to be exclusive, as suggested by the PCC values found (0.43–0.59, Figure 6). As mentioned above, Pearson correlation analysis generates values ranging from –1 to 1, where a value of 1 suggests full colocalization. In other words, these results suggest that the nanocarriers are within low-pH compartments. It should be noted that this finding seems to be in line with our previous study.[27,28] Ultrastructural analysis by TEM revealed that mPEO-*b*-PCL nanoparticles can be found both within vesicular structures and freely in the cytoplasm within Raw 264.7 macrophage-like cells.

To study the cellular internalization kinetics of the NPs within J774A.1 Mϕs, DACCA-labeled NPs (2 nmol $mL^{-1}$) were added to Mϕ monolayers and incubated for different times. Subsequently, the cellular uptake was analyzed using flow cytometry (**Figure 7**A). All of the obtained cell-associated fluorescence data were normalized to the maximum fluorescence values to ensure the comparability of the results determined from samples with variable total cell fluorescence intensities.[28]

As shown in Figure 7A, the fabricated NPs were successfully taken up by J774A.1 cells, and the cell-associated fluorescence intensity increased as the incubation time increased for all of the samples tested. A maximum cell fluorescence intensity was reached after 60–100 min of incubation (Figure 7A); the data were normalized to the plateau-corresponding values of fluorescence, individually. Subsequently, internalization half-time values (Figure 7A) were calculated based on the internalization time course by curve-fitting of the data using the following equation[49]

$$F(t) = F_0 + (F_{\text{plateau}} - F_0)\left(1 - e^{-tk}\right) \quad (2)$$

where $F(t)$ is the cell fluorescence signal at time $t$, $F_0$ and $F_{\text{plateau}}$ are the initial fluorescence signal and the maximum signal, respectively, and $k$ is the internalization rate constant. The half-time of internalization ($\tau_{1/2}$) was calculated as the ratio of ln 2 and $k$.

The cellular uptake of nanobeads, in general, depends on several factors, such as the size, charge, shape, and

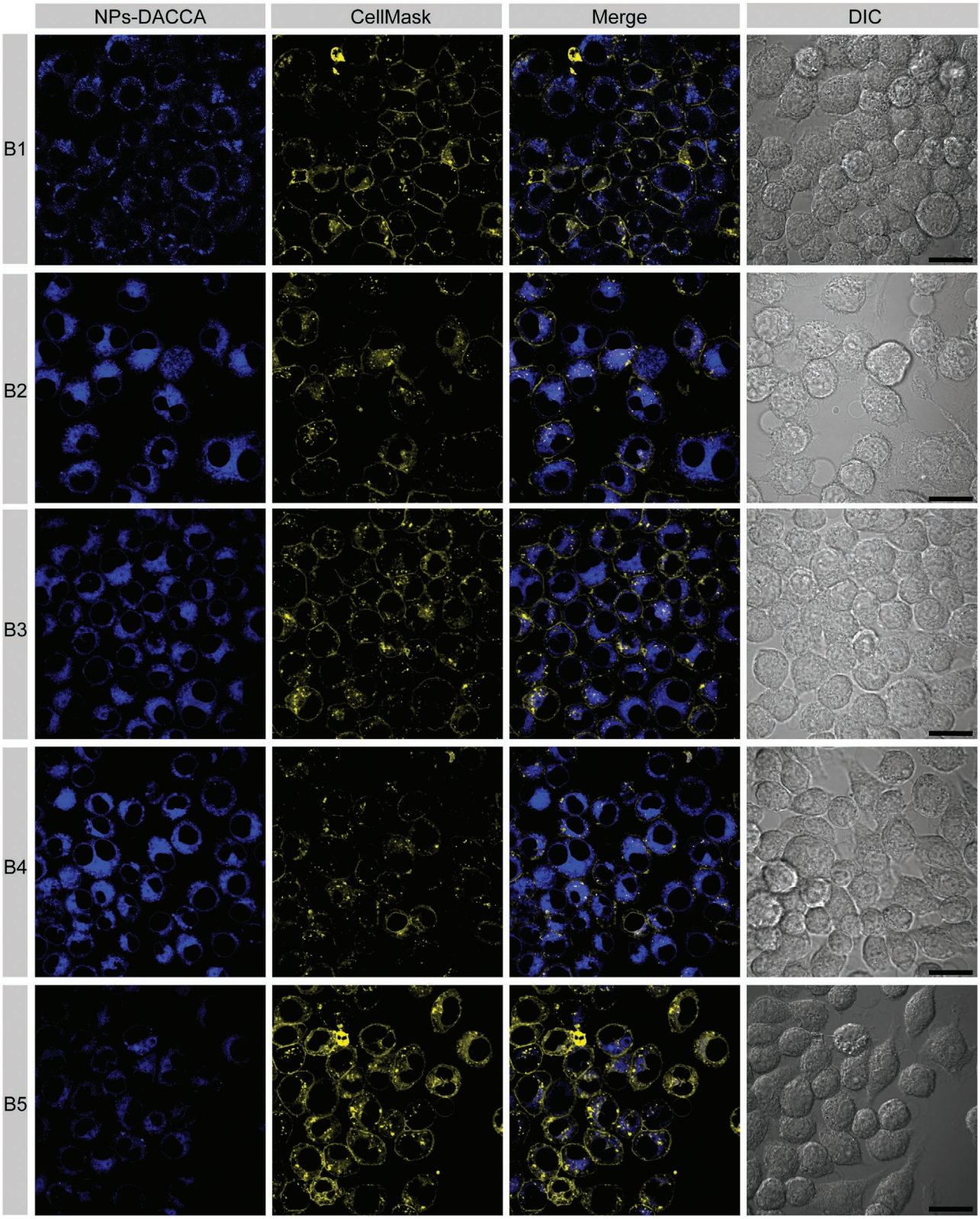


**Figure 5.** Study of DACCA-labeled NP uptake by J774A.1 cells. Fluorescence and differential interference contrast (DIC) images of J774A.1 cells are shown 40 min after the addition of DACCA-labeled NPs (2.8 nmol $mL^{-1}$, blue fluorescence). The plasma membrane-related CellMask Deep Red signal is pseudocolored in yellow. Scale bars: 20 µm.

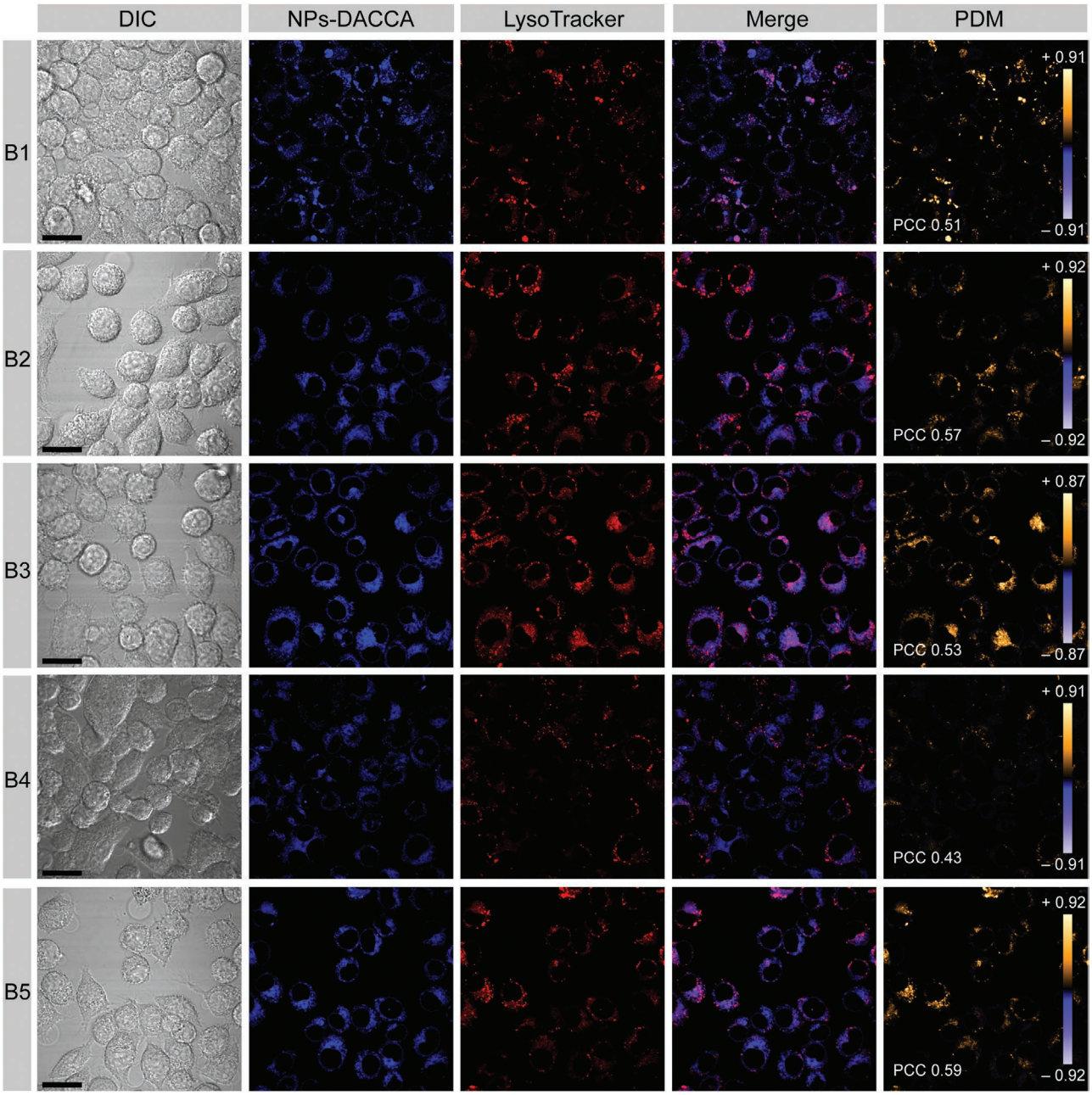


**Figure 6.** Study of DACCA-labeled NP localization within J774A.1 cells. CLSM images of J774A.1 M$\phi$s 40 min after the addition of DACCA-labeled NPs (2.8 nmol mL$^{-1}$) and LysoTracker. The analysis of colocalization was allowed by both the product of the differences from the mean (PDM) images and Pearson correlation coefficient (PCC) values. The PDM images are pseudocolored; each pixel is equal to the PDM value at that location and a PDM scale bar was inserted. The orange color indicates colocalized pixels and the blue color suggests segregation. Scale bars: 20 µm. DIC denotes differential interference contrast.

hydrophilic/hydrophobic ratio of the NPs.[42,50] Not surprisingly, the resulting uptake kinetics are then based on a combination of such parameters. Thus, a group of nanocarriers possessing several different variable properties makes interpretation of the kinetic results harder.[28] Despite this fact, the kinetics study carried out revealed a phenomenon worth mentioning; it was found that the P4HB-free mPEO$_{45}$-*b*-PCL$_{81}$-based sample **B1** exhibited a considerably high internalization $\tau_{1/2}$ value (≈54 min) compared to that of the rest of the samples analyzed.

Notably, the mPEO$_{45}$-*b*-(PCL$_{55}$-*co*-P4HB$_{19}$) copolymer (**B3**) exhibited an internalization $\tau_{1/2}$ of ≈9.5 min, even when having the same hydrophilic/hydrophobic ratio as that of **B1** as well as the same molecular weight. This may be due to the change in crystallinity and/or NP size, one of the main physicochemical aspects that influence cellular uptake. This finding suggests that the introduction of P4HB can strongly affect the biorelevant properties of such nanobead-based interventions. Such a hypothesis, however, must be investigated in

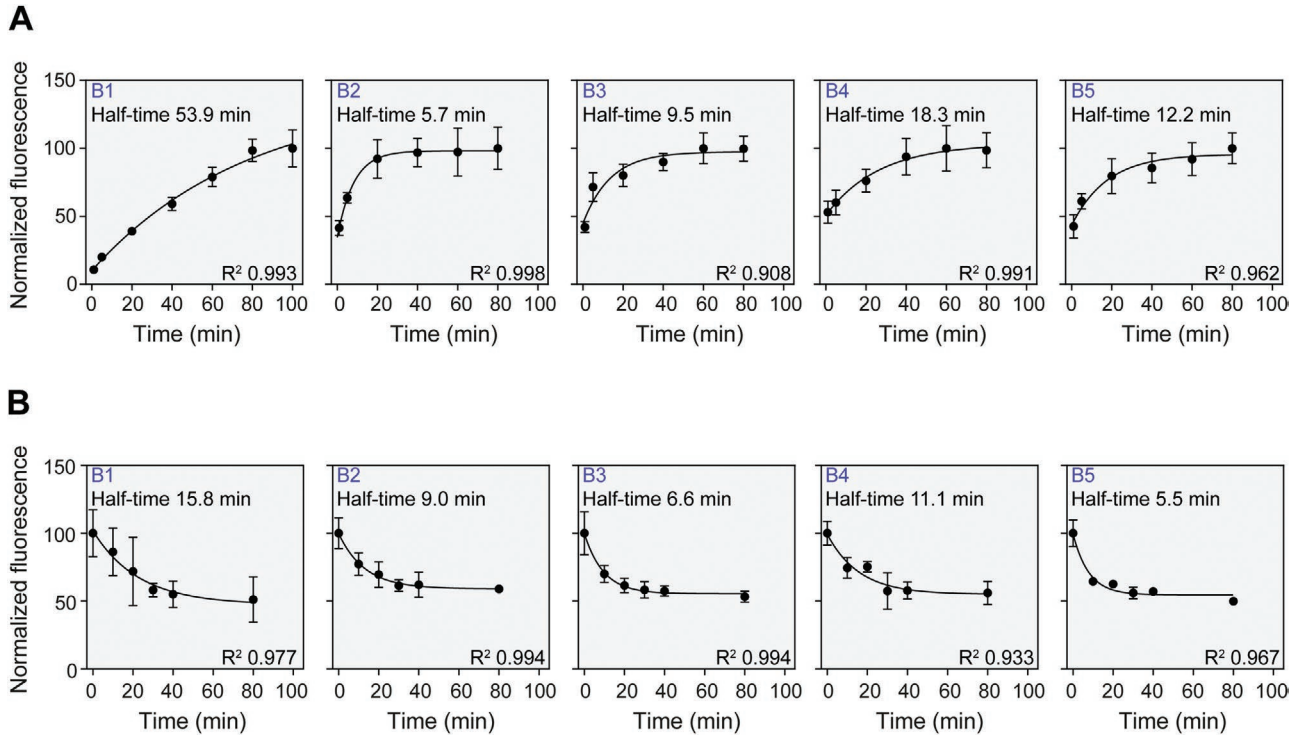


**Figure 7.** Study of DACCA-labeled NP fate. A) Time course of cell-associated fluorescence after the addition of 2 nmol mL$^{-1}$ DACCA-labeled formulations. The data were normalized to the maximum fluorescence values (i.e., the plateau values reached). B) Time course of NP degradation observed after the monolayers were incubated with 2 nmol mL$^{-1}$ DACCA-labeled formulations for 60 min. Both half-time and *R* squared values are shown. Note that **B1** exhibited different internalization as well as degradation kinetics compared to those of formulation **B3**, even when having the same hydrophilic/hydrophobic ratio as well as the same molecular weight.

more detail to come to any specific conclusions in terms of this phenomenon.

As mentioned above, a plateau in the cell-associated fluorescence was reached after 60–100 min of incubation with the DACCA-labeled formulations. Subsequently, a decrease in the cell-associated fluorescence values was observed (data not shown), as the enzymatic degradation of the DACCA-labeled matrix leads to quenching of its fluorescence.[27] Hence, to study the intracellular degradation kinetics, DACCA-labeled NPs (2 nmol mL$^{-1}$) were added to M$\phi$ monolayers and incubated for 60 min for each of the formulations tested. Subsequently, the cells were washed with PBS (i.e., time 0) and analyzed using flow cytometry at different time points (Figure 7B). The degradation rate constant values were determined by fitting the data to a single exponential decay model. The half-time of degradation was calculated as the ratio of ln 2 and the degradation rate constant.

In our recent study,[28] we suggested that there is a relationship between the lysosomal localization of a nanocarrier and its degradation kinetics in vitro. In other words, mPEO-*b*-PCL-based NPs with cytosolic localization within Raw 264.7 M$\phi$s exhibited slow intracellular degradation, and, vice versa, fast intracellular degradation was observed in the case of NPs colocalized with lysosomes, i.e., lipase-rich compartments.[51] It is evident from Figure 7B that all of the nanoformulations analyzed (i.e., **B1**, **B2**, **B3**, **B4**, and **B5**) revealed similar degradation patterns, probably because all of the samples exhibited similar colocalization within low-pH compartments. Similar to the uptake kinetics study, the P4HB-free sample **B1** was the most distinct, as it revealed the slowest degradation rate ($\tau_{1/2}$ of ≈16 min), which also suggests that the introduction of P4HB seems to be able to tune the biorelevant properties of the NPs. Similar to our recent study,[28] the flow cytometry results were not in line with the above-described $^1$H NMR degradation study. This is probably because the $^1$H NMR study was carried out in PBS only (i.e., without the presence of FBS or cell proteins), as protein-NP interactions play a crucial role in the biorelevant behavior. For the same reason, the flow cytometry results may be deemed to be more relevant, because they reflect interactions in biorelevant environments (i.e., in the presence of serum and intracellular proteins).

It is worth mentioning that enzymatic degradability suggests favorable behavior in vivo, as it can be assumed that the mPEO-*b*-(PCL-*co*-P4HB) copolymers undergo degradation to mPEO, 6-hydroxyhexanoic acid (the degradation product of PCL) and 4-hydroxybutyric acid. Both $mPEO_{44}$ (2000 Da) and $mPEO_{113}$ (5000 Da) do not exceed the threshold for the renal filtration of polymers 30–50 kDa.[52] The biocompatible 6-hydroxyhexanoic acid is converted to adipic acid by $\omega$-oxidation in the endoplasmic reticulum of liver and kidney cells in vivo. Adipic acid is then metabolized by $\beta$-oxidation and the Krebs cycle to carbon dioxide and water.[53] Similarly, 4-hydroxybutyric acid is a ubiquitous molecule in vivo, derived both endogenously and exogenously and is catabolized by processes including $\beta$-oxidation to acetyl-CoA and glycolate, $\alpha$-oxidation to 3-hydroxypropionate-CoA and formate, and cleavage of C-4 to yield 3-hydroxypropionate and carbon dioxide.[54]

## 4. Conclusions

The aim of this work was to describe, fundamentally characterize, and perform biorelevant analyses of biocompatible and biodegradable nanocarriers based on mPEO-*b*-(PCL-*co*-P4HB), where the γBL introduction would hopefully serve as a biorelevant behavior-controlling mechanism.

First, it has been shown that the copolymer composition of PCL-*co*-P4HB can be tuned not only by the feed ratio of the monomers but also by choosing a feasible catalyst. The difference in γBL incorporation was demonstrated when anionic or cationic catalysts were employed. A notable increase in incorporation was observed when anionic catalysis in a nonpolar environment were employed. The content of incorporated γBL was ≈30% when TBD was used as a catalyst of the copolymerization in toluene.

Additionally, we studied the biorelevant properties of P4HB-based nanocarriers. Their biocompatibility, cellular uptake, and degradation were evaluated. By combining flow cytometry and CLSM, we demonstrated that these nanocarriers can be internalized by macrophage-like cells in which the NPs underwent intracellular degradation. The influence of the presence of the γBL units on the biological behavior was observed. This method enabled control over the rate of degradation so that when the content of γ-butyrolactone increased, the rate of degradation increased.

Given our findings, this study provides a generalizable strategy for the future improvement of polyester nanobead-based interventions in application fields where fine-tuned properties are needed.

## Supporting Information

Supporting Information is available from the Wiley Online Library or from the author.

## Acknowledgements

Financial supports from the Czech Science Foundation (Grants Nos. 17-07164S and 17-09998S) the Ministry of Education, Youth and Sport of the Czech Republic (National sustainability program I, grant # POLYMAT LO1507) are gratefully acknowledged. T.U. and R.K. thank Dr. Sabina Nováková for her kind assistance with $^1$H NMR analysis. J.T. acknowledges support from Charles University (Project No. SVV260440) and would like to thank Dr. Tomáš Mazel for his expert flow cytometry data fitting advice and Dr. Jakub Hraníček (Department of Analytical Chemistry, Faculty of Science, Charles University) for his kindness in assisting with the instrumentation necessary for fluorescence spectroscopy. D.R. and M.S. acknowledge support from the Scientific Grant Agency VEGA and the Slovak Research and Development Agency (Project Nos. 2/0177/17 and 16-0550). The authors would like to thank Ewa Pavlova, who performed the TEM measurements.

## Conflict of Interest

The authors declare no conflict of interest.

## Author Contributions

T.U. synthesized the polymers, carried out the physicochemical characterizations of both the polymers and nanoparticles, and wrote the paper. J.T. carried out the cytotoxicity and confocal microscopy experiments and wrote the paper. D.R. performed the AF4 experiments. K.G. performed the flow cytometry investigations. R.K. performed and evaluated the $^1$H NMR analysis. M.Š. supervised the TEM investigations. M.S. supervised the AF4 experiments and evaluated the results. O.Š.J. supervised the flow cytometry investigations and cell-associated fluorescence data fitting. M.H. supervised the project and contributed to the final version of the paper.

## Keywords

biodegradation, macrophages, nanomedicine, nanoparticles, γ-butyrolactone

Received: November 28, 2019
Revised: January 22, 2020
Published online:

[1] V. P. Torchilin, *Pharm. Res.* **2006**, *24*, 1.
[2] R. Palao-Suay, L. G. Gómez-Mascaraque, M. R. Aguilar, B. Vázquez-Lasa, J. S. Román, *Prog. Polym. Sci.* **2016**, *53*, 207.
[3] I. Schlachet, J. Trousil, D. Rak, K. D. Knudsen, E. Pavlova, B. Nyström, A. Sosnik. *Carbohydr. Polym.* **2019**, *212*, 412.
[4] A. C. Albertsson, I . K. Varma, *Biomacromolecules* **2003**, *4*, 1466.
[5] P. Markland, V. C. Yang, *Encyclopedia of Pharmaceutical Technology*, Vol. *1,* 3rd ed. (Ed: J. Swarbrick), Informa Helthcare USA, New York **2007**.
[6] L. S. Nair, C. T. Laurencin, *Prog. Polym. Sci.* **2007**, *32*, 762.
[7] T. Moore, R. Adhikari, P. Gunatillake, *Biomaterials* **2005**, *26*, 3771.
[8] A. Nakayama, N. Kawasaki, S. Aiba, Y. Maeda, I. Arvanitoyannis, N. Yamamoto, *Polymer* **1998**, *39*, 1213.
[9] D. P. Martin, S. F. Williams, *Biochem. Eng. J.* **2003**, *16*, 97.
[10] P. Olsén, K. Odelius, A. C. Albertsson, *Biomacromolecules* **2016**, *17*, 699.
[11] D. Myers, A. Cyriac, C. K. Williams, *Nat. Chem.* **2015**, *8*, 3.
[12] W. H. Carothers, *Chem. Rev.* **1931**, *8*, 353.
[13] F. Korte, W. Glet, *J. Polym. Sci, Part B: Polym. Lett.* **1966**, *4*, 685.
[14] K. Yamashita, K. Yamamoto, J.-i. Kadokawa, *Chem. Lett.* **2014**, *43*, 213.
[15] M. Hong, E. Y.-X. Chen, *Nat. Chem.* **2015**, *8*, 42.
[16] M. Hong, E. Y.-X. Chen, *Angew. Chem., Int. Ed.* **2016**, *55*, 4188.
[17] N. Zhao, C. Ren, H. Li, Y. Li, S. Liu, Z. Li, *Angew. Chem., Int. Ed.* **2017**, *56*, 12987.
[18] L. Lin, D. Han, J. Qin, S. Wang, M. Xiao, L. Sun, M. Yuezhong, *Macromolecules* **2018**, *51*, 9317.
[19] C.-J. Zhang, L.-F. Hu, H.-L. Wu, X.-H. Cao, X.-H. Zhang, *Macromolecules* **2018**, *51*, 8705.
[20] P. Walther, W. Frey, S. Naumann, *Polym. Chem.* **2018**, *9*, 3674.
[21] Y. Shen, Z. Zhao, Y. Li, S. Liu, F. Liu, Z. Li, *Polym. Chem.* **2019**, *10*, 1231.
[22] M. Hong, X. Tang, B. S. Newell, E. Y. X. Chen, *Macromolecules* **2017**, *50*, 8469.
[23] P. Walther, S. Naumann, *Macromolecules* **2017**, *50*, 8406.
[24] N. Dolan, D. P. Gavin, A. Eshwika, K. Kavanagh, J. McGinley, J. C. Stephens, *Bioorg. Med. Chem. Lett.* **2016**, *26*, 630.
[25] L. Luo, J. Tam, D. Maysinger, A. Eisenberg, *Bioconjugate Chem.* **2002**, *13*, 1259.
[26] S. Petrova, D. Klepac, R. Konefał, S. Kereïche, L. Kováčik, S. K. Filippov, *Macromolecules* **2016**, *49*, 5407.
[27] J. Trousil, S. K. Filippov, M. Hrubý, T. Mazel, Z. Syrová, D. Cmarko, S. Svidensk, J. Matějková, L. Kováčik, B. Porsch, R. Konefał, R. Lund, B. Nyström, I. Raškab, P. Štěpánek, *Nanomedicine* **2017**, *13*, 307.

[28] J. Trousil, Z. Syrová, N.-J. K. Dal, D. Rak, R. Konefał, E. Pavlova, J. Matějková, D. Cmarko, P. Kubíčková, O. Pavliš, T. Urbánek, M. Sedlák, F. Fenaroli, I. Raška, P. Štěpánek, M. Hrubý, *Biomacromolecules* **2019**, *20*, 1798.
[29] M. Bauer, C. Lautenschlaeger, K. Kempe, L. Tauhardt, U. S. Schubert, D. Fischer, *Macromol. Biosci.* **2012**, *12*, 986.
[30] P. Ralph, M. A. Moore, K. Nilsson, *J. Exp. Med.* **1976**, *143*, 1528.
[31] *Biological Evaluation of Medical Devices – Part 5: Tests for In Vitro Cytotoxicity*, International Organization for Standardization, Geneva, Switzerland **2009**.
[32] A. Duda, S. Penczek, P. Dubois, D. Mecerreyes, R. Jérôme, *Macromol. Chem. Phys.* **1996**, *197*, 1273.
[33] M. Danko, J. Mosnáček, *Polimery* **2017**, *62*, 272.
[34] A. Bhaw-Luximon, D. Jhurry, S. Motala-Timol, Y. Lochee, *Macromol. Symp.* **2005**, *231*, 60.
[35] M. Dionzou, A. Morère, C. Roux, B. Lonetti, J. D. Marty, C. Mingotaud, P. Joseph, D. Goudounèche, B. Payré, M. Léonettie, A.-F. Mingotaud, *Soft Matter.* **2016**, *12*, 2166.
[36] R. F. Domingos, M. A. Baalousha, Y. Ju-Nam, M. M. Reid, N. Tufenkji, J. R. Lead, G. G. Leppard, K. J. Wilkinson, *Environ. Sci. Technol.* **2009**, *43*, 7277.
[37] O. Sedlacek, B. D. Monnery, S. K. Filippov, R. Hoogenboom, M. Hruby, *Macromol. Rapid Commun.* **2012**, *33*, 1648.
[38] S. Agarwal, X. Xie, *Macromolecules* **2003**, *36*, 3545.
[39] A. Ianiro, J. Patterson, Á. González García, M. M. J. van Rijt, M. M. R. M. Hendrix, N. A. J. M. Sommerdijk, I. K. Voets, A. C. C. Esteves, R. Tuinier, *J. Polym. Sci., Part B: Polym. Phys.* **2018**, *56*, 330.
[40] S. Zolls, R. Tantipolphan, M. Wiggenhorn, G. Winter, W. Jiskoot, W. Friess, A. Hawe, *J. Pharm. Sci.* **2012**, *101*, 914.
[41] M. Ukawala, T. Rajyaguru, K. Chaudhari, A. S. Manjappa, S. Pimple, A. K. Babbar, R. Mathur, A. K. Mishra, R. S. Murthy, *Drug Delivery* **2012**, *19*, 155.
[42] Z. Zhang, Q. Qu, J. Li, S. Zhou, *Macromol. Biosci.* **2013**, *13*, 789.
[43] K. Kolouchova, O. Sedlacek, D. Jirak, D. Babuka, J. Blahut, J. Kotek, M. Vit, J. Trousil, R. Konefał, O. Janouskova, B. Podhorska, M. Slouf, M. Hruby, *Biomacromolecules* **2018**, *19*, 3515.
[44] P. Grossen, D. Witzigmann, S. Sieber, J. Huwyler, *J. Controlled Release* **2017**, *260*, 46.
[45] P. Grossen, G. Québatte, D. Witzigmann, C. Prescianotto-Baschong, L.-H. Dieu, J. Huwyler, *J. Nanomater.* **2016**, *2016*, 13.
[46] J. Jin, B. Sui, J. Gou, J. Liu, X. Tang, H. Xu, Y. Zhang, X. Jin, *PLoS One* **2014**, *9*, e112200.
[47] Y. Pei, Y. Yeo, *J. Controlled Release* **2016**, *240*, 202.
[48] S. M. Abaza, *Parasitol. United J.* **2016**, *9*, 1.
[49] I. Vainshtein, L. K. Roskos, J. Cheng, M. A. Sleeman, B. Wang, M. Liang, *Pharm. Res.* **2015**, *32*, 286.
[50] S. Behzadi, V. Serpooshan, W. Tao, M. A. Hamaly, M. Y. Alkawareek, E. C. Dreaden, D. Brown, A. M. Alkilany, O. C. Farokhzad, M. Mahmoudi, *Chem. Soc. Rev.* **2017**, *46*, 4218.
[51] M. J. Czaja, A. M. Cuervo, *Autophagy* **2009**, *5*, 866.
[52] M. E. Fox, F. C. Szoka, J. M. J. Fréchet, *Acc. Chem. Res.* **2009**, *42*, 1141.
[53] A. Orchel, K. Jelonek, J. Kasperczyk, Z. Dzierzewicz, *Acta Pol. Pharm.* **2010**, *67*, 710.
[54] S. Sadhukhan, G.-F. Zhang, G. P. Tochtrop, *ACS Chem. Biol.* **2014**, *9*, 1706.